

2

WL-TR-93-1023

AD-A263 563



ATMOSPHERIC TRANSVERSE COHERENCE  
LENGTH MEASUREMENT SYSTEM FOR  
LASER COMMUNICATIONS



GARY D. WILKINS  
COMMUNICATIONS TECHNOLOGY GROUP  
SYSTEM AVIONICS DIVISION

FEBRUARY 1993

Final Report for the Period September 1989 - July 1992



Approved for Public release; distribution is unlimited.

AVIONICS DIRECTORATE  
WRIGHT LABORATORY  
AIR FORCE MATERIEL COMMAND  
WRIGHT-PATTERSON AIR FORCE BASE OHIO 45433-7409

93 4 30 021

93-09298


5402

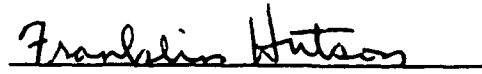
# NOTICE

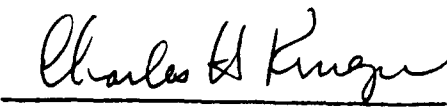
When Government drawings, specifications, or other data are used for any purpose other than in connection with a definitely Government-related procurement, the United States Government incurs no responsibility or any obligation whatsoever. The fact that the government may have formulated or in any way supplied the said drawings, specifications, or other data, is not to be regarded by implication, or otherwise in any manner construed, as licensing the holder, or any other person or corporation; or as conveying any rights or permission to manufacture, use, or sell any patented invention that may in any way be related thereto.

This report is releasable to the National Technical Information Service (NTIS). At NTIS, it will be available to the general public, including foreign nations.

This technical report has been reviewed and is approved for publication.

  
GARY D. WILKINS

  
FRANKLIN T. HUTSON, Chief  
Communications Technology Section  
System Avionics Division

  
CHARLES H. KRUEGER, Chief  
System Avionics Division  
Avionics Directorate

If your address has changed, if you wish to be removed from our mailing list, or if the addressee is no longer employed by your organization please notify WL/AAAI-2, WPAFB, OH 45433-7301 to help us maintain a current mailing list.

Copies of this report should not be returned unless return is required by security considerations, contractual obligations, or notice on a specific document.

# REPORT DOCUMENTATION PAGE

Form Approved  
OMB No. 0704-0188

Public reporting burden for this collection of information is estimated to average 1 hour per response, including the time for reviewing instructions, searching existing data sources, gathering and maintaining the data needed, and completing and reviewing the collection of information. Send comments regarding this burden estimate or any other aspect of this collection of information, including suggestions for reducing this burden, to Washington Headquarters Services, Directorate for Information Operations and Reports, 1215 Jefferson Davis Highway, Suite 1204, Arlington, VA 22202-4302, and to the Office of Management and Budget, Paperwork Reduction Project (0704-0188), Washington, DC 20503.

1. AGENCY USE ONLY (Leave blank)		2. REPORT DATE FEB 93	3. REPORT TYPE AND DATES COVERED FINAL 09/01/89--07/31/92	
4. TITLE AND SUBTITLE ATMOSPHERIC TRANSVERSE COHERENCE LENGTH MEASUREMENT SYSTEM FOR LASER COMMUNICATIONS			5. FUNDING NUMBERS PE 61101 PR ILIR TA 00 WU 01	
6. AUTHOR(S) GARY D. WILKINS				
7. PERFORMING ORGANIZATION NAME(S) AND ADDRESS(ES) AVIONICS DIRECTORATE WRIGHT LABORATORY AIR FORCE MATERIEL COMMAND WRIGHT-PATTERSON AFB OH 45433-7409			8. PERFORMING ORGANIZATION REPORT NUMBER WL-TR-93-1023	
9. SPONSORING/MONITORING AGENCY NAME(S) AND ADDRESS(ES) AVIONICS DIRECTORATE WRIGHT LABORATORY AIR FORCE MATERIEL COMMAND WRIGHT-PATTERSON AFB OH 45433-7409			10. SPONSORING/MONITORING AGENCY REPORT NUMBER WL-TR-93-1023	
11. SUPPLEMENTARY NOTES				
12a. DISTRIBUTION/AVAILABILITY STATEMENT  APPROVED FOR PUBLIC RELEASE: DISTRIBUTION IS UNLIMITED.			12b. DISTRIBUTION CODE	
13. ABSTRACT (Maximum 200 words)  THIS PAPER SUMMARIZES THE WRIGHT LABORATORY IN-HOUSE LABORATORY INDEPENDENT RESEARCH (ILIR) CONDUCTED TO DETERMINE THE FEASIBILITY OF USING INHERENT INFORMATION, SUCH AS ANGLE-OF-ARRIVAL FLUCTUATIONS OF INCIDENT RADIATION AND SPREADING OF THE FOCUSED SPOT SIZE, OBTAINED THROUGH THE MEASUREMENT OF THE DIFFRACTION LIMITED APERTURE OF THE ATMOSPHERE ( $r_o$ ), TO ADAPTIVELY OPTIMIZE LASER COMMUNICATIONS SYSTEM PARAMETERS. THE SYSTEM DEVELOPED TO MEASURE THE $r_o$ AND DETAILS CONCERNING THE 8 KILOMETER PULSED LASER COMMUNICATIONS LINK ESTABLISHED BETWEEN THE WRIGHT-PATTERSON AFB TREBEIN TEST SITE AND AREA B, BUILDING 620, LASER COMMUNICATIONS LABORATORY (LCL) ARE DESCRIBED.				
14. SUBJECT TERMS LASER COMMUNICATIONS CHARGE COUPLED DEVICE OPTICAL COMMUNICATIONS			15. NUMBER OF PAGES 53	
ANGLE-OF-ARRIVAL ATMOSPHERIC TURBULENCE TRANSVERSE COHERENCE LENGTH			16. PRICE CODE	
17. SECURITY CLASSIFICATION OF REPORT UNCLASSIFIED	18. SECURITY CLASSIFICATION OF THIS PAGE UNCLASSIFIED	19. SECURITY CLASSIFICATION OF ABSTRACT UNCLASSIFIED	20. LIMITATION OF ABSTRACT UL	

# Contents

LIST OF ILLUSTRATIONS.....	iv
LIST OF TABLES .....	iv
ACKNOWLEDGMENTS .....	v
1 Introduction .....	1
2 Background .....	4
2.1 Objective of the LCL In-House Research Effort .....	7
2.2 Approach .....	7
3 Equipment Design and Development .....	8
3.1 Atmospheric Transverse Coherence Length Measurement System .....	8
3.2 Communications Equipment .....	14
3.2.1 Transmitter .....	14
3.2.2 Receiver .....	15
4 Bit Error Rate Testing .....	16
5 Data .....	21
5.1 $r_o$ Data .....	22
5.2 BER Data .....	23
5.3 Meteorological Data .....	24
5.4 Data Analysis .....	25
6 Observations and Conclusions .....	30
7 Future LCL Efforts .....	34
8 Summary .....	35
Appendix Equipment Specifications .....	37
Bibliography .....	48

DTIC Q-1111-17 UNCLASSIFIED 6

Accession For	
NTIS CRA&I	<input checked="" type="checkbox"/>
DTIC TAB	<input type="checkbox"/>
Unannounced	<input type="checkbox"/>
Justification .....	
By .....	
Distribution / .....	
Availability Codes	
Dist	Avail and/or Special
A-1	

## LIST OF ILLUSTRATIONS

<u>FIGURE</u>	<u>TITLE</u>	<u>PAGE</u>
1	Atmospheric Turbulence Profile.....	2
2	Rotating Reticle Wheel Method of Measuring $r_0$ .....	6
3	Free Space Laser Communications Link .....	7
4	$r_0$ Measuring System .....	9
5	Intensity Distribution of a Received Laser Signal.....	12
6	Gray Scale Normalized Disk Intensity Distribution.....	13
7	Laser Communications Receiver Equipment.....	16
8a	Transmitted Laser Communications Signal.....	18
8b	Received Communications Signal With Scintillation Effects.....	18
9	Time Variations Caused by Scintillation Induced Fluctuations of the Laser Communications Signal.....	19
10	Horizontal Location of the Focused Spot on the CCD vs. Time...	25
11	Bit Error Rate vs. Time for 19 June 1991.....	25
12	Visibility vs. Time for 19 June 1992.....	28
13	Exposure Length vs. Time for 19 June 1992.....	28
14	Positioning of a Round Airy Disk on a Square Detector.....	30

## LIST OF TABLES

<u>TABLE</u>	<u>TITLE</u>	<u>PAGE</u>
5-1	Example Output Data From The $r_0$ Measurement System	22
5-2	Example Format of Collected Meterological Data	24
5-3	BER versus Source Corellation Coefficients for 19 June 1992 Average Hourly Observations	26

## **ACKNOWLEDGMENTS**

Thank you to Mr. Michael J. Findler, summer hire Doctoral candidate at Arizona State University for the exceptional programming accomplished on this project while working in the WL Laser Communications Laboratory under the Air Force Office of Scientific Research Graduate Student Research Program during the summer of 1990, and for the work he accomplished as a private contractor during the summer of 1991. Also, thank you to Mr. Franklin Hutson, Captain Ronald Wallace, Captain Ricky Shute and Mr. Joung C. Ha for the time they invested in editing this document to ensure its quality.

## 1 Introduction

One of the most important items to consider when using free space laser communications in an atmospheric environment is the atmosphere. Whether communication is from air-to-air or air-to-ground, the atmosphere plays a major role in corrupting it. Moisture, aerosols, temperature and pressure changes produce refractive index variations in the air by causing random variations in density. These variations, depicted in Figure 1, are referred to as eddies and have a lens effect on light passing through them. When a plane wave passes through these eddies, parts of it are refracted randomly causing a distorted wavefront with the combined effects of variation of intensity across the wavefront and warping of the isophase surface. By the time the light reaches its destination, it is no longer spatially or temporally coherent over the entire wavefront, and an optical system sampling a large portion of the wavefront would not be able to focus the light to the diffraction limit of the optics. Instead, the size of the Airy disk (ref Eugene Hecht, Optics page 419) produced would be a function of the diffraction limited aperture of the atmosphere, or atmospheric transverse coherence length,  $r_0$ , as it is sometimes called. An optical system which has an aperture equal to or less than the  $r_0$  will sample a coherent portion of the wave and produce an image that is based upon the quality of the optical equipment. If the aperture of the optical equipment is larger than the  $r_0$ , then the quality of the image will be dependent upon the amount of atmospheric turbulence in the optical path.

Since optical communications relies on the use of wavelengths which are highly influenced by changes in refractive index, we decided to investigate the direct relationship between atmospheric turbulence and communications quality. The reason for doing this was to see if enough information could be gathered by repeated sampling of the  $r_0$  to allow changes to be made in the communications parameters which would optimize the communications and guarantee maximum information throughput.

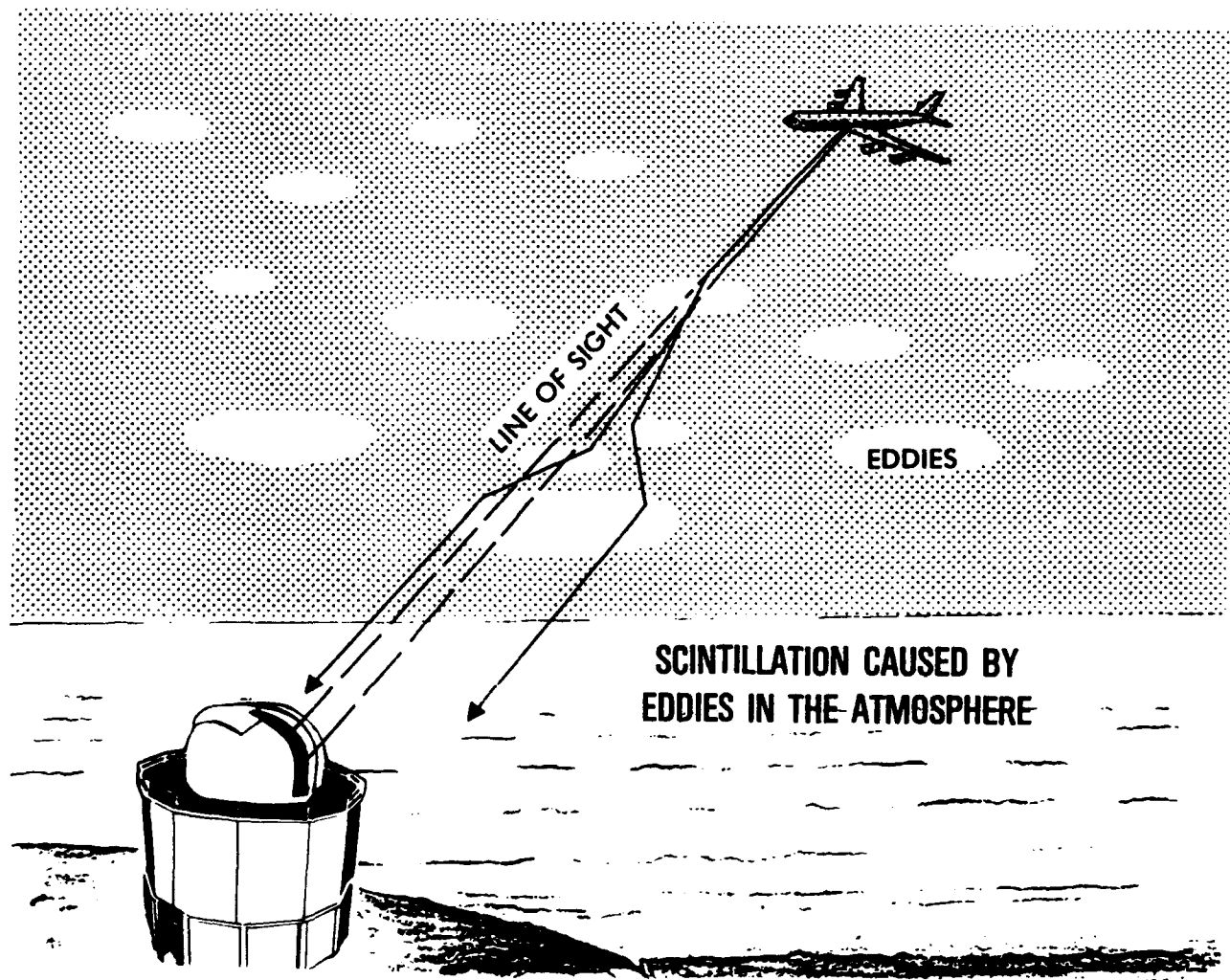


Figure 1 Atmospheric Turbulence Profile



Our approach to obtaining our goal involved setting up a laser communications link over a 5-mile path and measuring the Bit Error Rate (BER) of the digital signal, and measuring the  $r_o$  of the path. To accomplish this, a few minor details had to be taken care of first. Since there were no laser communications systems available off-the-shelf which satisfied our requirements for an 8-kilometer free-space link, we built a laser transmitter, a receiver, the required interfaces and the  $r_o$  measuring equipment in the laboratory with available off-the-shelf components and equipment.

Since publication of the software developed to drive the CCD camera and measure the  $r_o$  would limit the distribution of this Technical Report to the Government, it is not being published in this report. However, if any one in the government has a need for the software, it can be obtained from the author at WL/AAAI-2. A limited distribution publication of the software is planned in the near future.

## 2 Background

One of the earliest methods of determining  $r_0$  involved photography. Light from a distant star was focused onto a photographic plate and after a suitable exposure time the plate was developed. The diameter of the focused spot was then determined with the aid of a densitometer and a mechanical measuring device. The  $r_0$  was then calculated in accordance with diffraction theory and the following equations which relate the telescope aperture,  $D$ , the wavelength of light,  $\lambda$ , and the focal length of the optical system,  $f.l.$ , to the size of the focused spot, Airy disk diameter:

$$\text{AiryDiskDiameter} = 2.44(\lambda * f.l.) / D \quad 2-1$$

Knowing that using an optical system with an aperture greater than the  $r_0$  will produce a focused spot size which is dependent upon the diffraction limited aperture of the atmosphere allows us to replace the telescope aperture,  $D$ , in the diffraction equation with  $r_0$  to arrive at a relationship between the Airy Disk Diameter and  $r_0$ :

$$r_0 = \frac{2.44(\lambda * f.l.)}{(\text{AiryDiskDiameter})} \quad 2-2$$

Even though one could conceivably use an automatic camera to take a sequence of pictures over a period of time, it would be a rather slow process and in no way could it be considered close to a real-time measurement. As interest in the stochastic nature of the atmosphere grew and technology advanced, other methods of measuring the "seeing condition" of the atmosphere were developed.

A past endeavor of mine involved developing a method of measuring the  $r_0$  for use as a tool to help characterize the atmosphere for surveillance applications. I used a 1-meter aperture cassegrain telescope, shown in Figure 2, to gather incoming light from a point source and focus it onto a spinning reticle wheel which contained a track of apertures which increased geometrically in size (ref. Wilkins RADC-TR-86-192). Light passing through the apertures of

the reticle was collected by a photomultiplier tube and the resulting electrical signal was digitized by an analog-to-digital converter. The digital output contained information about the modulation transfer function of the atmosphere and was reduced by computer to provide the diffraction limited aperture of the atmosphere. The system was large, even without the 1-meter telescope, and the optics were difficult to keep aligned due to atmospheric turbulence induced beam wander. Although the system was good for its time, its size and mechanical parts were impractical for use as a real time atmospheric turbulence monitor for laser communications systems.

Other methods of obtaining the  $r_0$  have also been employed. One such method is to measure the refractive index structure parameter,  $C_n^2$ , using a stellar scintillometer. This method involves taking several scintillation measurements along the optical path and deriving the  $C_n^2$  information analytically. The  $r_0$  can then be obtained by using an equation which relates  $r_0$  to  $C_n^2$ . Although this method does arrive at the  $r_0$ , it was not considered acceptable for our laser communications work because it is time intensive. Ostensibly, atmospheric conditions change due to wind, temperature and pressure changes. Consequently, the atmospheric refractive index structure parameter and thus the diffraction limited aperture of the atmosphere also undergo constant change. Since, using the  $C_n^2$  method requires several scintillation measurements and analytical computations for each  $r_0$  measurement, it is not possible to derive the  $r_0$  fast enough to make the required communications parameter changes to allow for an optimum communications channel.

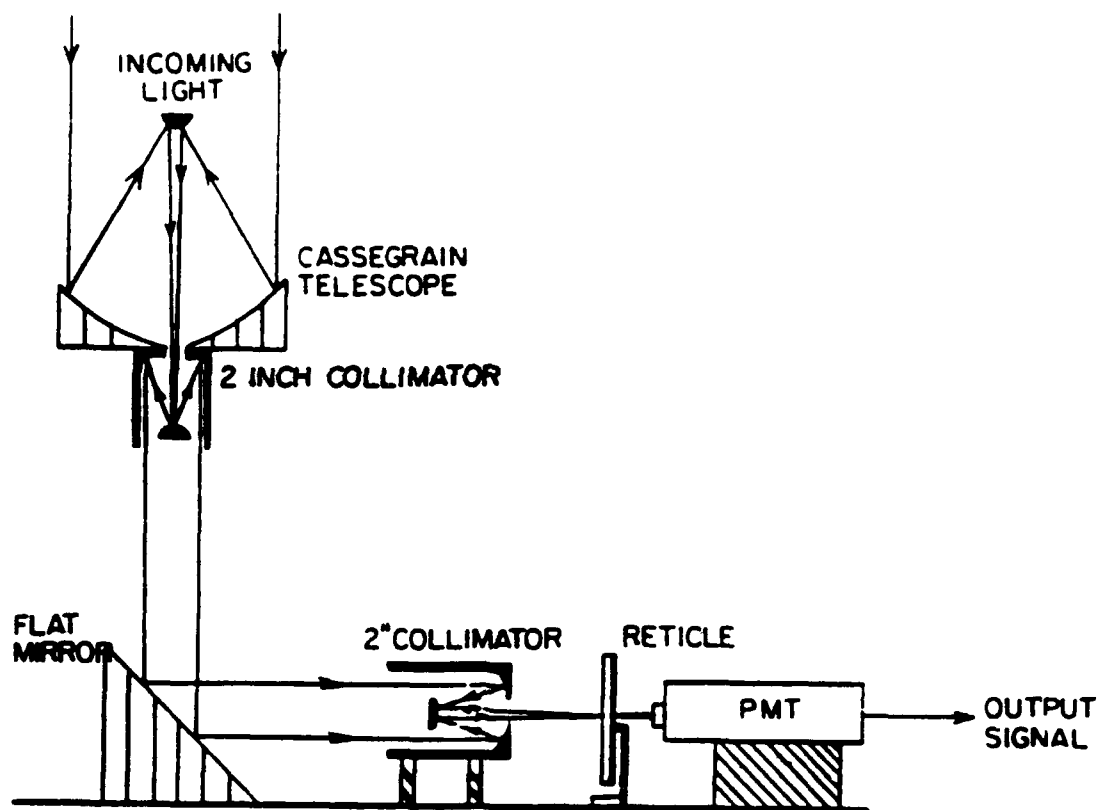


Figure 2. Rotating Reticle Wheel Method of Measuring  $r_0$ .

## 2.1 Objective of the LCL In-House Research Effort

The purpose of this In-House Laboratory Independent Research (ILIR) project was to conduct research to determine the feasibility of using inherent information obtained through the measurement of the diffraction limited aperture of the atmosphere ( $r_0$ ) to adapt laser communications system parameters to provide an optimum communication channel in the presence of atmospheric turbulence.

## 2.2 Approach

To accomplish the objective, an 8 kilometer pulsed laser communications link has been established between Trebein Test Site and the Laser Communications Lab (LCL) on the Wright-Patterson AFB, Area B, Building 620 tower, twelfth floor, as shown in Figure 3. The laser transmitter and Bit Error Rate encoder are located at the Trebein site and the receiver,  $r_0$ , meteorological, and data acquisition equipment are in the LCL. Since  $r_0$  measuring equipment and laser receivers are not available off the shelf, they were designed and built in-house. The remainder of this technical report will focus on the design of the  $r_0$  measurement device, the lasercom transmitter and receiver and the data collected.

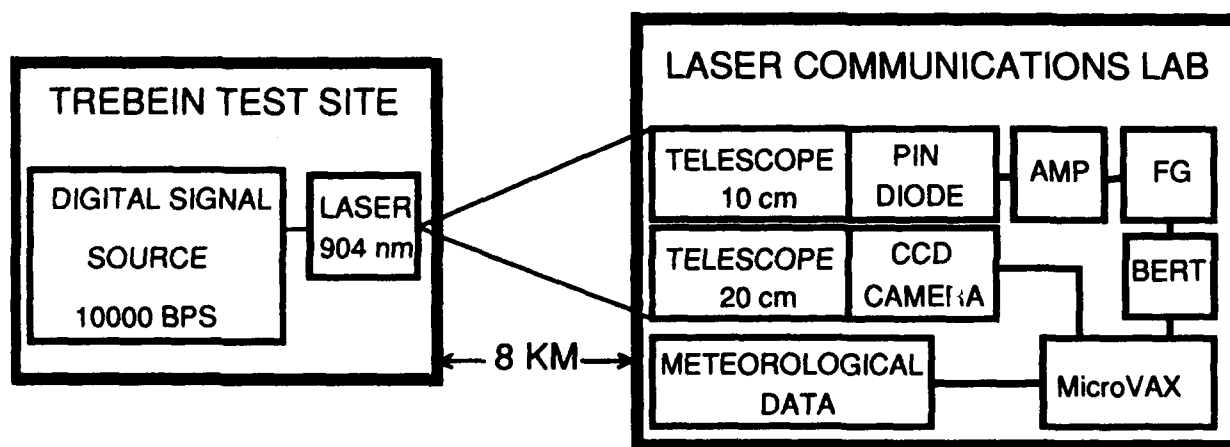


Figure 3. Free Space Laser Communications Link

### 3 Equipment Design and Development

Because free-space laser communications is still in its infancy, some of the equipment required for this project was not available off-the-shelf and had to be designed and built in-house. This section describes the design of the  $r_o$  and communications equipment.

#### 3.1 Atmospheric Transverse Coherence Length Measurement System

The LCL houses the equipment used for measuring the  $r_o$ . An in-house designed and built system, the device incorporates the simplicity of the photographic method with the data acquisition capability of the rotating reticle wheel method, without the need for chemicals or mechanical devices. The system consists of a Celestron 20 cm aperture telescope which focuses the light from the laser onto a VIDEK camera CCD array as shown in Figure 4. The hardware platform for the system includes the following:

1. Celestron Classic 8 Schmidt Cassegrain Telescope
2. VIDEK MEGAPLUS 1024 by 1024 CCD array camera
3. Digital Equipment Corporation VAXstation II/GPX computer with:
  - a) Dual RX50 floppy disk drive
  - b) TK50 tape drive
  - c) RD54 159 megabyte hard disk drive
  - d) RD53 71 megabyte hard disk drive
  - e) Univision Digitizer / Display Controller (UDC-500Q) with an Intel 82786 graphics coprocessor.
4. VR290 color monitor
5. LK201 keyboard
6. Sampo high resolution, 19-inch monochrome monitor.
7. A 904-nm center wavelength, 10-nm bandpass interference filter

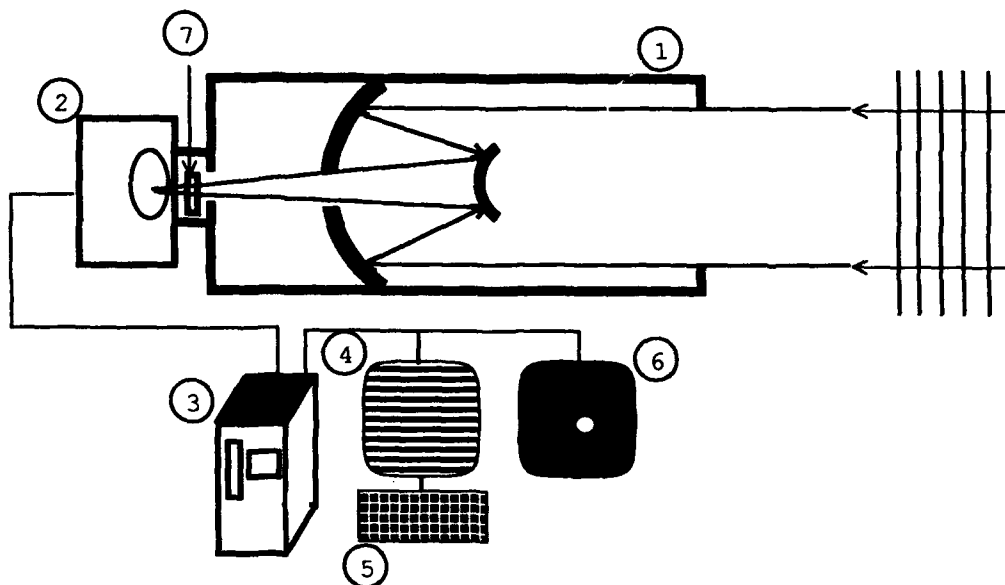


Figure 4.  $r_0$  Measuring System

The image of the Fourier transform of the incoming laser light captured by the round aperture telescope (1), and CCD camera (2) is digitized by a Univision UDC500Q frame grabber residing inside the MicroVAX computer (3). Horizontal and vertical sync pulses are delivered to the camera and digital video is delivered to the UDC-500Q controller via a 37-pin D connector mounted on the UDC-500Q. Images are displayed on the high resolution Sampo monitor (6) connected directly to the UDC-500Q video output connector.

Some computer code required by the frame grabber to digitize the camera output and display the image was supplied by Univision as part of the UDC500 demonstration package. Although several demo programs were supplied, the only one required to operate the camera was UDC500\_VAXUTL.EXE. Upon execution of the program, the input required from the user is:

**COMMAND****DESCRIPTION**

C 2	CAMERA TYPE SELECTION (VIDEK)
T 12	INITIALIZE 82786 BIU & DP REGISTERS
T 18	GRAB THE IMAGE
T 17	SNAP AN IMAGE

Command T 18 places the UDC500 in a continuous frame grabbing mode with the frame rate being dependent upon the shutter delay and exposure settings on the rear of the VIDEK camera. The image output is displayed on a Sampo high resolution (1024 by 1024) monitor. Executing command T 17 then freezes the image for further processing such as determining object size and position on the screen.

The Videk camera and UDC500Q display controller were purchased as a set, complete with demonstration software, from Univision Inc. The software, UDC500Q, and VIDEK camera displayed the images beautifully on the high resolution (1024 by 1024) monitor. However, the system had one very serious drawback. It would continuously snap pictures frame after frame without allowing for shutter/exposure control. The camera itself has the following modes of operation which are switch selectable at the rear of the camera:

**MODE****DESCRIPTION**

0	Shutter closed, remote control of the mode lines
1	Shutter locked open, continuous video output
2	Shutter locked open, triggered internally
3	Shutter locked open, manually triggered
4,5	Continuous shutter opening and closing
6	Shutter and exposure controlled manually
7	Shutter and exposure controlled by computer

Modes 5 and 6 cause the camera to continuously snap pictures at the rate of approximately two pictures per second. The length of exposure can be varied from 14 msec to 240 msec using the camera exposure adjustment potentiometer. When the Videk camera was connected to the UDC500Q and the UDC500\_VAXUTL.EXE program initiated with the C2 (Videk camera se-



lection) and T 12 and T 18 commands, the camera would continuously snap pictures as though it were in mode 5 or 6. Each of the camera modes was tried with the frame grabber and software, but the result was always the same. Univision was contacted and their only explanation was that all of their boards exhibit the same behavior. Since the fast drive times and inability to control the exposure did not meet the requirements for the project, and Univision would not provide the source code used to drive the camera, LCL personnel decided to diagnose the problem by analyzing the Videk camera, UDC500, and their specifications.

The problem was obvious from the start. The pinout assignments for the video connector on the back of the Videk camera, as listed in Table 2-3 of the Videk Operator Manual, did not all correspond to the pinout assignments given in paragraph 2.4.3 of the UDC500Q user's manual. Specifically, the Videk manual states that pin 19 is the MC2 control and pin 37 is the MC1 control, and Univision switched them on their output connector. This switch caused the Videk camera to enter mode 5 and continuously take pictures. Although the interface configuration could have been intentional to allow the camera to be turned on by the software, but internally self-controlled, it was not acceptable for our application. Since the camera was being used to monitor atmospheric turbulence under varying conditions of visibility, on a minute-by-minute basis, the continuous picture taking state of the camera was unacceptable because the time and length of exposure needed to be controlled. Also, since the shutter was only guaranteed by Videk to operate 2,000,000 times, it would potentially need replacing after each 11.5 days of data gathering.

Once the cause of the continuous picture snapping was determined, there still remained the task of determining how new software could be written to control the exposure of the camera. By experimentally turning on different bits in the UDC500 address and monitoring which control lines were affected, a method was developed which allowed the MC1 control line of the UDC500Q to act as the VIDEK MC2 control line, and the UDC500Q MC2 line to accomplish the function of the MC1 control line. Once this was accomplished, software was written which

allowed the camera to trigger on queue and the exposure to be varied from the minimal allowable exposure of the camera, 14 milliseconds, to as long as the operator desires.

Sampling time was another crucial consideration in the development of the software for the system. Over exposure to the laser radiation caused blooming of the CCD array in the vertical direction. This reduces the resolution and prevents measurements of the Airy disk diameter in the vertical direction from being used in the  $r_0$  calculation. Also, since the intensity is non-uniformly distributed across the Airy disk as seen in Figure 5, under exposure could lead to measurement errors if the diameter of the disk was measured at the wrong intensity level, i.e., near the peak versus the bottom of the irradiance curve. Ideally, the most accurate approach would be to measure the diameter of the first zero in the Fourier transform. However, since much of the field sampled by the CCD array is at least the same intensity as the first minima of the diffraction pattern, accomplishing this would be more time consuming and counterproductive than accepting a small error and measuring the diameter of the disk at an intensity just above that of the first spurious disk.

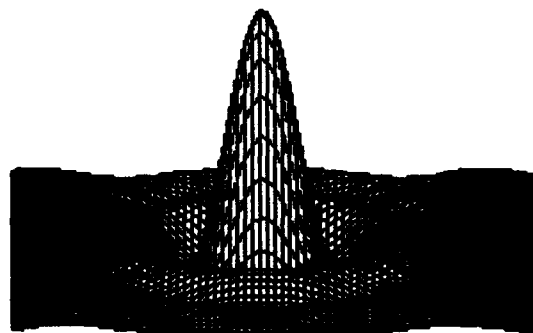


Figure 5. Intensity Distribution of a Received Laser Signal

To properly estimate the amount of time required for the sample exposure, we developed the software to initially accept a guess from the operator and then either increment or decrement by 10-millisecond steps until an acceptable intensity level was reached. By acceptable intensity level, it is meant that there must be at least 1 pixel, and not more than 100 pixels, on the screen that are white. Since the UDC500Q has the capability of digitizing the image to 256 levels of gray, with 0 corresponding to black and 255 corresponding to white, the computer merely increments until there are enough pixels in the acceptable range of 245 to 255. Increasing the exposure too long can actually turn the whole screen white causing measurement error. This is the reason we put a limit on the number of white pixels in the acceptable range. Any more than 100 pixels means that the CCD array is severely blooming, or the background light is stronger than the laser energy. In that case, the computer resets the initial time to 100 milliseconds and starts reincrementing in order to get to the acceptable level. Once an acceptable exposure is achieved, the diameter of the Airy disk is measured just above the first spurious disk at an intensity level of 50. This is shown in the computer generated gray scale Sinc function graph of Figure 6.

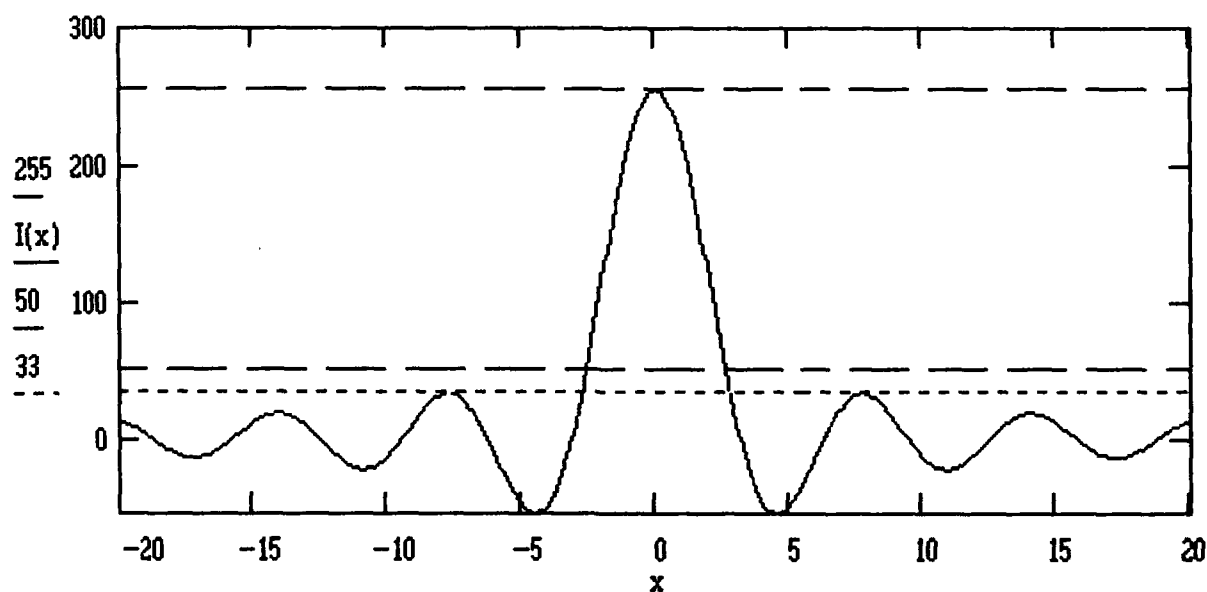


Figure 6. Gray Scale Normalized Airy Disk Intensity Distribution

Extremely turbulent days can cause blooming on one frame exposure, and an underexpo-

sure on the next frame. In order to keep the CCD blooming to a minimum, the vertical diameter of the Airy disk is compared to the horizontal diameter. If the vertical diameter exceeds the horizontal diameter by more than 5 pixels, the software decrements the exposure time by 5 milliseconds after the third consecutive reading reporting the vertical diameter is out of range. Since underexposure causes the diameter of the disk to be measured too close to the top of the curve, the same method was used. If three consecutive measurements are made in which there are no pixels in the white range (245-255), the exposure is incremented by 10 milliseconds. Three consecutive bad readings were determined by experimentation to provide an optimal amount of time to determine if the exposure really needed to be changed or not. Less than three causes the system to bounce back and forth between exposure levels causing an unacceptable number of bad readings.

### 3.2 Communications Equipment

The equipment used for the data communications portion of the project consisted of an off-the-shelf laser transmitter, an in-house built receiver and off-the-shelf pattern generator/error detector equipment for measuring the quality of the communications link.

#### 3.2.1 Transmitter

The laser transmitter is a Laser Diode, Inc. LT-201 capable of 100 watts peak optical output power, but was operated at 20 watts peak for this experiment. It operates at a room temperature wavelength of 904 nanometers and a beam divergence of 1 milliradian. The transmitter is edge triggered by the return to zero TTL output of a bit error rate encoder operating at a clock frequency of 10-kHz and emits a 40-nanosecond pulse for each positive transition of the data input signal. A Hewlett Packard (HP) H96 5245L Electronic Counter slaved to an Arbiter Systems Satellite Controlled Clock provided the 10-kHz synchronized clock. The maximum pulse repetition frequency of the LT-201 has been determined by laboratory experimentation to be 16,800 pulses per second. Technical specifications for the LT-201, as well as other major

equipment used for the receiver and  $r_0$  measurement system are provided in the Appendix.

### 3.2.2 Receiver

The laser receiver was designed and built in-house. It consists of Celestron 90mm Maksutov Cassegrain spotter scope(1), depicted in Figure 7, adapted to focus the incoming laser radiation onto a silicon photodiode(2), housed with a 10 nm bandpass filter(3) in a Melles Griot modular photodetection system(4). A Melles Griot 13AMP005 Wide Bandwidth Detector Amplifier(5) supplies current to the detector and acts as the first stage amplifier. The signal is then amplified by a Stanford Research Systems Model SR560 low noise amplifier(6), which supplies the needed gain and electronic filtering. The resulting 40-microsecond Gaussian shaped pulses are converted into TTL level square pulses with a Tektronix FG507 function generator(7) and subsequently fed into an HP 3780A Bit Error Rate Tester (8) for analysis. A Hewlett Packard crystal controlled counter (9), slaved to an Arbiter Systems Inc. 1026B Satellite controlled clock(10), provided the 10,000 Hz needed by the BERTs for the synchronous data stream.

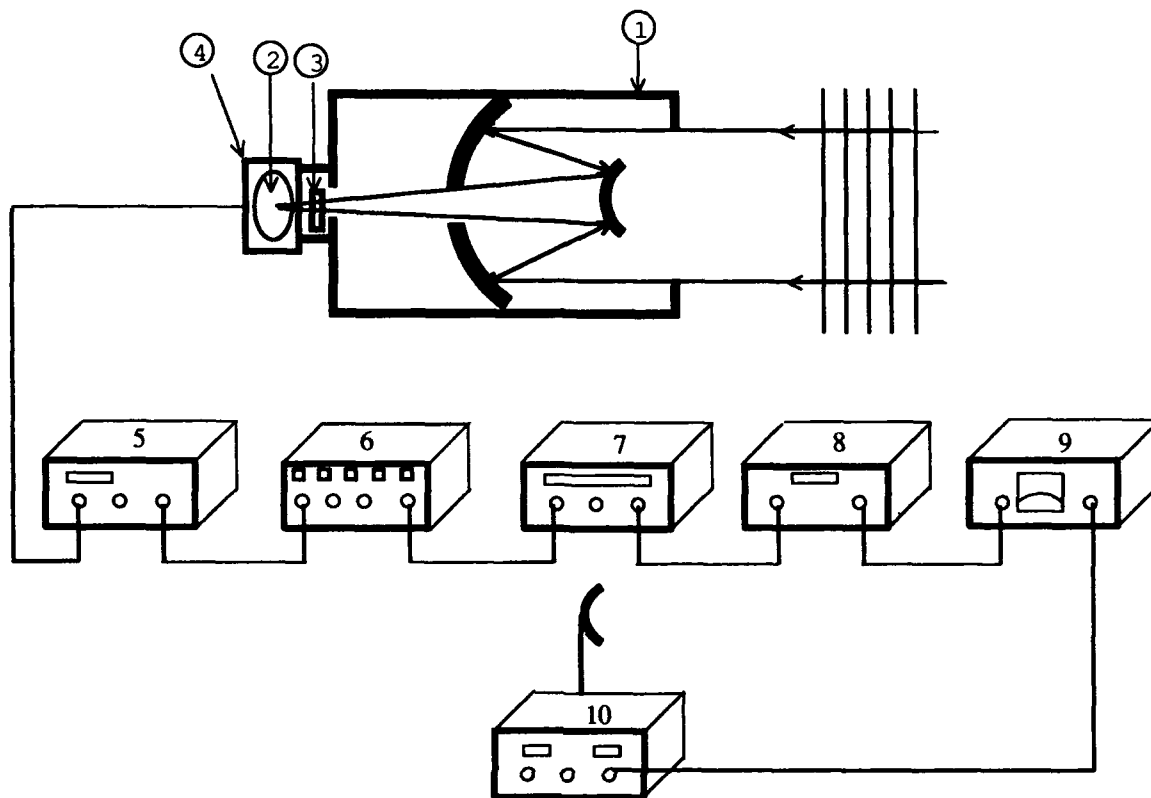


Figure 7. Laser Communications Receiver Equipment

#### 4 Bit Error Rate Testing

Two HP 3780A Pattern Generator / Error Detectors were used to measure the quality of the communications link. One HP 3780A was interfaced with the LT-201 laser transmitter at the Trebein Test Site and the second HP 3780A was interfaced with the in-house built receiver in the LCL as seen in Figure 7. Since the LT-201 laser transmitter is edge triggered from the leading edge of a TTL pulse, the interface for the transmitter was fairly straightforward since the data output of the HP 3780A can be configured to provide a Return to Zero, (RZ), TTL data format. One problem which needed to be overcome, however, was that the internal clock rate

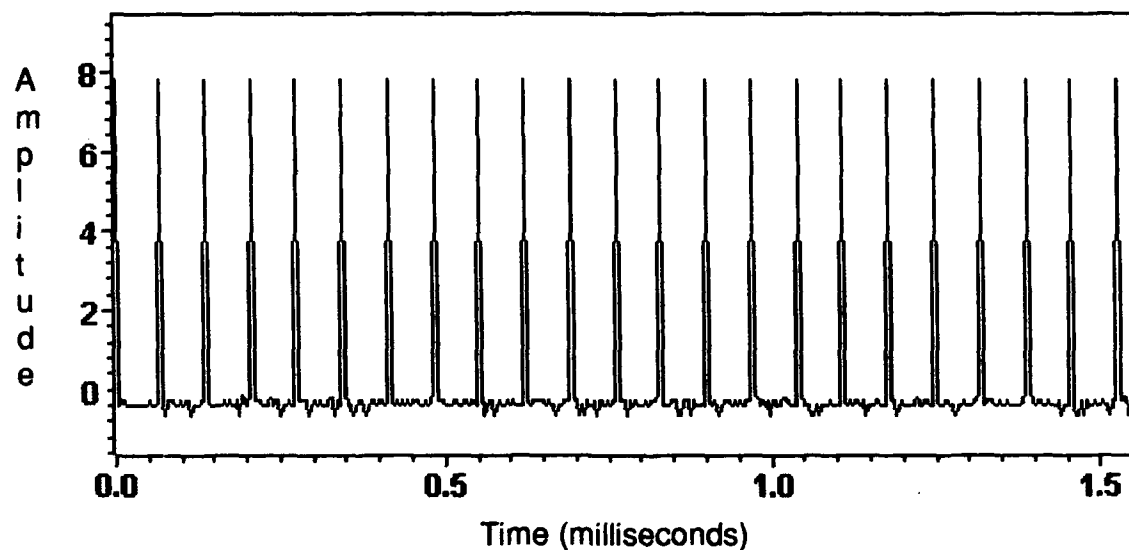
of the HP 3780A is 10 Mega pulses per second. This greatly exceeds the maximum transmission rate of LT-201 laser transmitter 16.8 Kilo pulses per second. To conquer this situation, the 10-kHz output of an Hp crystal controlled clock was connected to the external clock inputs of the HP 3780A at both the transmitter and receiver ends of the link.

Once the output of the receiver was interfaced with the the HP 3780A in the LCL, and the system was turned on, it became evident that there were still a few more problems to be solved. Since the clock of the system was now decreased to 0.001 of the internal clock speed of the HP 3780A, it took 1000 times longer to update the BER information on the read-out, or 1 minute and 40 seconds. On calm, nonturbulent days with the diffraction limited aperture of the atmosphere approaching the diameter of the telescope, the BERT would sync almost long enough to provide a reading and then give a SYNC LOSS signal. After a comparison was accomplished on the two external clocks, it was discovered that one clock differed from the other by 1 clock pulse every 1 minute and 30 seconds. From this, it was determined that there was no possible way of conducting the BER test without synchronizing the clocks more thoroughly at each end of the link.

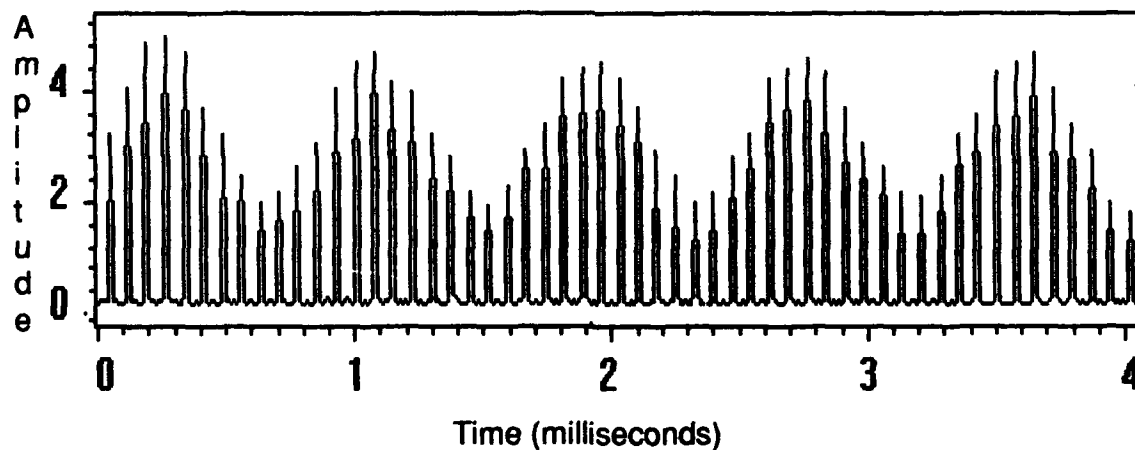
Since we were unable to get 2 cesium standards for use to synchronize the transmitter to the receiver, a different approach was taken. Two Arbiter Systems Inc. 1026B Satellite Controlled Clocks were set up, in the LCL and Trebein Test Site, to receive the satellite-disseminated time code from a National Bureau of Standards Geostationary Operational Environmental Satellite (GOES). Since the time code is transmitted once every half-second, the 1 MHz clock output has an accuracy of 1 in  $10^7$ . This helped tremendously. The transmitter and receiver BERTs synchronized and the BER data collection process started.

After all of the equipment induced problems had been solved and the data collection process started, there remained one last challenge, the atmosphere. Scintillation caused by the random movement of the eddies in the atmosphere cause the input signal at the receiver to vary in am-

plitude from a constant peak amplitude as shown in Figure 8a to that in Figure 8b.



(a)



(b)

Figure 8 a) Transmitted Laser Communications Signal, b) Received Communications Signal With Scintillation Effects

The challenge then becomes one of scintillation induced frequency jitter. At the receiver, the received 40-microsecond pulses are converted back into 5-volt TTL compatible pulses by using a function generator. After the received signal has been amplified and filtered by a



Stanford Research Systems model SR560 Low Noise Preamplifier, it is fed into the trigger input of the function generator where the leading edge of the pulse causes the function generator to output one TTL compatible pulse of preset duration for every Gaussian shaped pulse of a certain preset minimum amplitude at the input. Since the amplitude of the input pulses are not constant and have a certain amount of rise and fall time, and the voltage at which the function generator is set to trigger is constant, triggering is accomplished at different relative amplitude levels for each input pulse. For instance, a pulse that has made it through the atmosphere with minimal scintillation effect might appear such as pulse P1 in Figure 9 and key the transmitter at time  $t_1$ , or 50 percent of its maximum amplitude. On the other extreme, a pulse that is severely hampered by scintillation may not even trigger the function generator until it has almost reached its maximum amplitude, such as pulse P2, at time  $t_2$ . The net result is a TTL output with a random time interval between pulses. Since the transmit BERT is synchronized with the receive BERT, the receive BERT expects to see pulses at a certain time with very little variance. If this time interval varies by too much, the receive BERT gets confused as to which pulse it is trying to read, and eventually gives up and dumps its data and starts a new cycle.

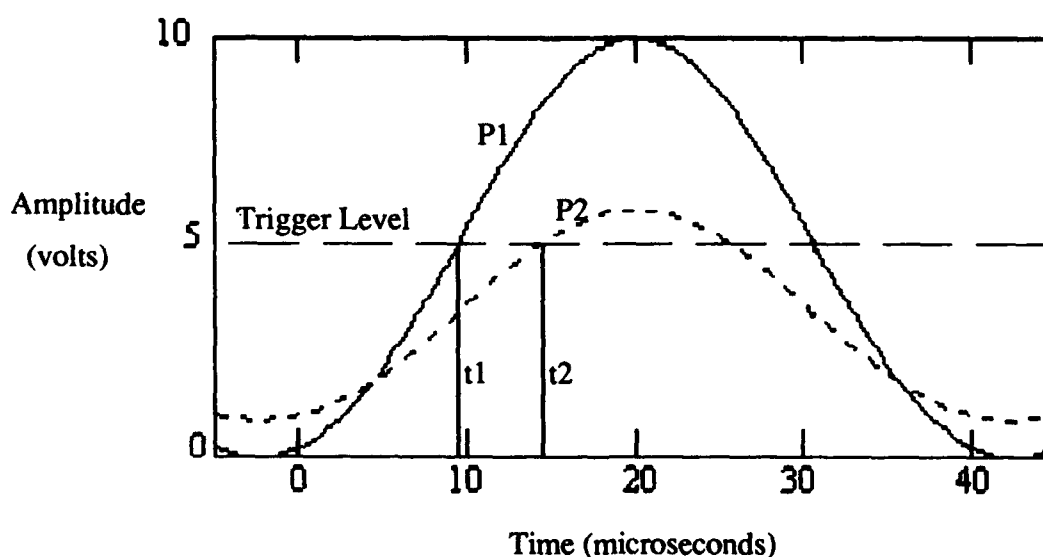


Figure 9. Time Variations Caused by Scintillation Induced Intensity Fluctuations of the Laser Communications Signal

Pulse-to-pulse timing variations as large as 30 microseconds, corresponding to intensity fades as large as 36 dB, were observed during the data collection process. In order to get the BERT to collect data, a great deal of tweaking of the amplifier gain and function generator trigger level was required to find an acceptable level which resulted in minimal pulse-to-pulse time variations. An amplifier with automatic gain control to level out the fades and provide a constant signal amplitude would have been extremely useful on this project. A function generator which triggered at the peak amplitude could have been equally as effective. Unfortunately, we were unable to locate such devices, so we accomplished as much data collection as possible.

## 5 Data

Meteorological, BER, and  $r_0$  data were collected around the clock from 15 June 1992 to 21 June 1992, barring occasional outages due to inclement weather. The observation rates among the different types of data differ because of equipment limitations, so extra care was required during the evaluation phase. Since the BER data were limited to the 1-minute 40-second output cycle of the BERT, and the  $r_0$  data collection rate of an average of one sample every 9.5 seconds was dependent upon the run time of the computer algorithm, more  $r_0$  data were collected than BER data. To ensure that the BER data corresponded to  $r_0$  data collected during the same time interval, all the  $r_0$  data collected during each BERT cycle were averaged. Since meteorological data were collected at 1-minute intervals, and it did not vary nearly as much as the  $r_0$  and BER data, the values for temperature, relative humidity and atmospheric pressure were chosen to correspond to the time at which the BERT had completed approximately half of its cycle.

Visibility was a particular concern because some of the problems were man-made and could not be explained as easily as relative humidity variations. After designing and building the receiver and  $r_0$  measurement system, setting up the communications link, and solving the BER equipment synchronizing problem, we were ready to collect data. The very day we began collecting data, a contractor broke ground to build a new department store right under our communications link. The amount of dust placed in the atmosphere between the transmitter and receiver sites was unbelievable. During the hours the contractor was working, the visibility decreased from beyond 7 to less than 5 miles, and the exposure length of the  $r_0$  measurement system increased from 250 milliseconds to greater than 2 seconds. Correlation of the  $r_0$  data with BER data over a whole day gave some very depressing results. For the 19th of June, the correlation coefficient  $r$  was only 0.189 which resulted in a coefficient of determination,  $r^2$ , of only 0.03576. However, since so much data existed over the 7-day collection, it was decided to use only that data collected between the hours of 8 P.M. and 8 A.M. which corresponded to a visibility of at least 7 miles, in order to isolate the  $r_0$  effects on BER from the effects of visibility

on BER. The following sections detail the type of data collected, the correlation process and the results.

## 5.1 $r_0$ Data

The rate at which  $r_0$  data was collected is a function of the amount of time it takes for the computer algorithm to snap an image using the camera, collect and analyze the data, and log the data to the hard drive. The data collection portion of the algorithm is highly dependent upon the visibility of the atmosphere which causes a longer exposure length for decreased visibility. The result is observations which vary in time from one every 8 seconds to one every 11 seconds for exposure lengths of 20 milliseconds to 1 second, respectively. Approximately 60,480  $r_0$  data points were collected during the week.

The collected data are logged directly to the computer hard disk in ASCII format. It contains information on the horizontal and vertical size, exposure length pixel location information for the right most and bottom most pixels. Table 5-1 is an example of the collected data format. The  $r_0$  data are available directly from the data base as seen in Table 5-1, and it is also printed to the computer monitor after each sample. Angle-of-arrival information is stored in pixel location format to allow for a post data collection qualitative analysis of the condition of the  $r_0$  measurement system during the data collection phase. The horizontal and vertical angle-of-arrival (HAOA and VAOA) of the incident radiation, relative to the direction the optical receiver is pointed, can be determined via the following relationship:

$$\text{HAOA} = \text{Optical FOV} * (\text{Right Pixel} - \text{Horizontal Diameter} / 2) / 1023 \quad 5-1$$

$$\text{VAOA} = \text{Optical FOV} * (\text{Bottom Pixel} - \text{Vertical Diameter} / 2) / 1023 \quad 5-2$$

Table 5-1 Example Output Data From the  $r_o$  Measurement System

Time (H:M:S)	Diameter Horizontal (cm)	Diameter Vertical (cm)	Exposure (msec)	Right Pixel	Bottom pixel	$r_o$ (cm)
12:22:33	22	16	150	488	501	2.948877
12:22:44	28	19	150	481	517	2.316975
12:22:54	22	18	150	484	503	2.948877
12:23:05	22	24	150	486	511	2.948877
12:23:16	16	18	150	488	507	4.054706
12:23:27	23	21	150	491	505	2.820665
12:23:38	21	17	150	483	506	3.089300
12:23:49	22	17	150	486	497	2.948877
12:23:59	20	21	150	483	508	3.243765
12:24:10	14	12	150	483	501	4.633950
12:24:21	21	18	150	488	500	3.089300
12:24:32	18	14	150	486	502	3.604183
12:24:43	21	14	160	483	504	3.089300
12:24:54	20	18	160	489	505	3.243765
12:25:04	20	16	160	484	502	3.243765
12:25:15	22	19	160	482	503	2.948877
12:25:26	20	21	160	483	504	3.243765
12:25:37	13	11	160	479	505	4.990407
12:25:48	21	24	170	489	509	3.089300

## 5.2 BER Data

Because of the reduced clock rate mentioned in Section 4 above, BER data were collected at a rate of one sample every 1 minute, 40 seconds and resulted in 6,048 data points over the 7-day collection period. The largest impediment against the successful collection of BER data was that of synchronizing the transmitter to the receiver. After that problem was solved, the data

collection process was dependent upon visibility, scintillation, and aerosol scattering. There was no special format used for the data logging process. An HP printer was connected to the printer port of the BERT and the BER and time were printed at the end of each cycle. The data were then manually entered into a computer spreadsheet for analysis.

### 5.3 Meteorological Data

Relative humidity, temperature and atmospheric pressure data were collected at the rate of one sample per minute over the testing period resulting in another 30,240 data points. The data samples, collected by sensors located outside the LCL, are digitized using a Qualemetrics QDL2000 Data Logger and stored on the hard disk of an IBM compatible Personal Computer (PC) in ASCII format. Table 5-2 is an example of the data format.

Table 5-2. Example Format of Collected Meteorological Data

<b>Station #</b>	<b>Battery Voltage (volts)</b>	<b>Time (H:M:S)</b>	<b>Temperature (degrees F)</b>	<b>% Relative Humidity</b>	<b>Atmospheric Pressure (inches Hg)</b>
99	014.6	09:20:00	83.25	80.25	29.10
99	014.7	09:21:00	83.27	81.21	29.12
99	014.8	09:22:00	83.28	80.87	29.11
99	014.6	09:23:00	83.31	80.58	29.11
99	014.4	09:24:00	83.29	81.03	29.13
99	014.5	09:25:00	83.30	81.00	29.12
99	014.6	09:26:00	83.28	80.63	29.13

In addition to the meteorological data collected in the LCL, the base provided hourly observations of wet and dry bulb temperatures, wind speed and visibility. The observations were taken approximately 1 mile east of the laser communications link and do not totally reflect the meteorological conditions along the communications path. However, they do provide a rough

indication of the conditions present during the data collection process.

#### 5.4 Data Analysis

Because the results of evaluating a whole day's worth of data in one analysis led to such a low coefficient of determination, these data were first averaged over the hour it was collected to provide a grand mean by hour to allow for some data snooping to uncover gross inconsistencies. One of the major problems discovered during the analysis process involves angle-of-arrival changes of the incident laser radiation. Since the  $r_o$  measurement system we developed was given the ability to track the position of the focused light on the CCD detector, it was a fairly simple task to correlate BER data with focused light position data. Figure 10 is a plot of horizontal location of the focused light on the CCD camera detector versus the hour of the day, and Figure 11 is a plot of BER versus hour of the day for 19 June 1992. The resultant correlation coefficients,  $r$ , and coefficients of determination,  $r^2$ , are tabulated in Table 5-3.

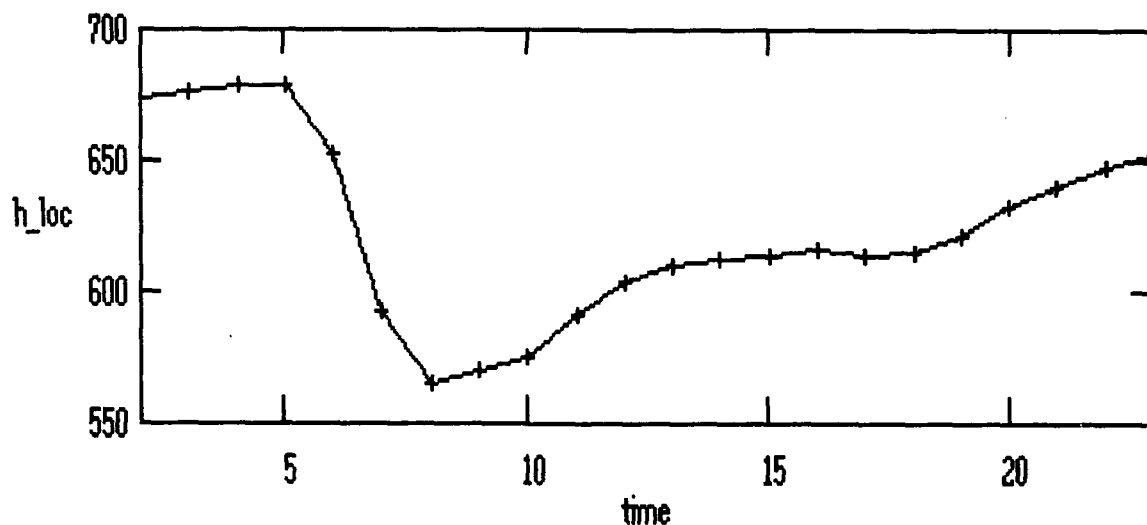


Figure 10. Horizontal Location of the Focused Spot on the CCD (pixels) vs. Time (EST)

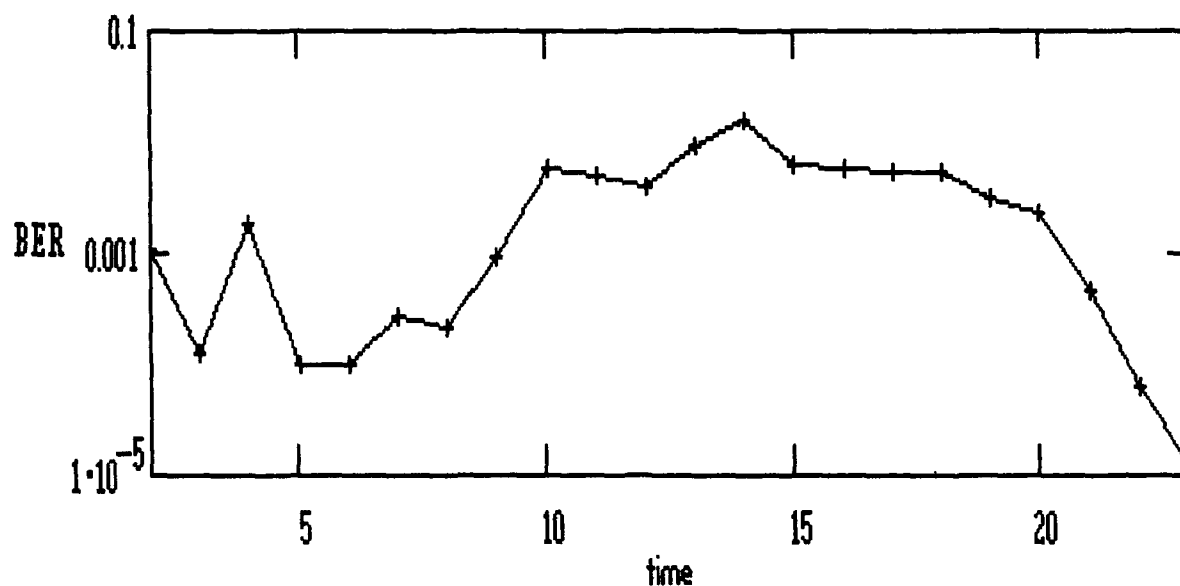


Figure 11. Bit Error Rate vs. Time (EST) for 19 June 1991

Table 5-3 BER versus Source Correlation Coefficients for 19 June 1992 Average Hourly Observations

source	r	r <sup>2</sup>
vertical location	-0.3339	0.1115
horizontal location	-0.6048	0.3657
r <sub>o</sub>	0.1891	0.0358
visibility	-0.6316	0.3989
exposure length	0.5698	0.3247
Temperature	0.7194	0.5173

Almost 37 percent of the variability can be explained by the horizontal location of the focused spot on the CCD camera detector. What appears to be happening is the wave front of the



THIS  
PAGE  
IS  
MISSING  
IN  
ORIGINAL  
DOCUMENT

27-11

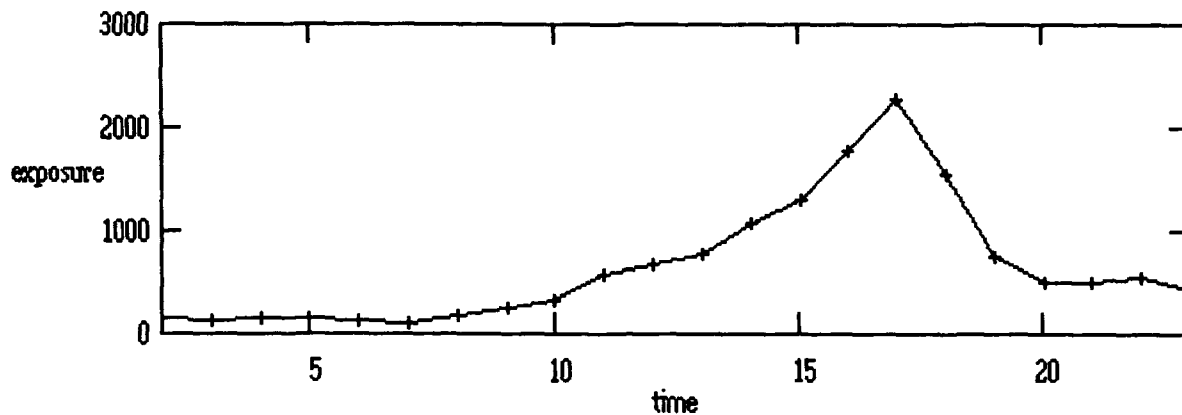


Figure 13. Exposure Length (milliseconds) vs. Time (EST) for 19 June 1992

With two of the largest sources of variation in BER explained, it was decided to look at the data only between the hours of 8 P.M. and 6 A.M. Eastern Standard Time (EST) since those were the hours least affected by platform movement/angle-of-arrival changes. In addition, the data for this period were filtered to eliminate all data corresponding to an exposure length greater than 150 milliseconds which relates to a visibility of less than 7 miles. After the filtering process, the  $r_0$  data were averaged over the 1-minute 40-second BERT cycles and correlated over various finite periods. The results ranged from uncorrelated data to several periods where the coefficients of determination exceeded 0.4 with a minimum of 28 degrees of freedom. The best correlation coefficient achieved during the testing was -0.70538 with 27 degrees of freedom and a corresponding coefficient of determination of 0.4978, indicating that as much as 49.78 percent of the variance in BER was attributed to the  $r_0$  for that period.

## 6 Observations and Conclusions

The data we obtained contain some very interesting observations which should be taken into consideration by laser communications developers. Most of the time, the data collected behaved as one might think it should. An increase in  $r_o$  would cause an increase in the quality of the received signal, and there would be a corresponding low BER. However, there were also cases contrary to this. On several occasions, the BER actually went up (signal quality went down) with increasing  $r_o$ . The explanation for this behavior involves the situation of platform movement. An optimum signal is achieved when the size of the Airy disk is equal to or less than the active area of the detector as depicted in Figure 14a. A decrease in  $r_o$  will cause an increase in the size of the Airy disk and eventually some of the energy contained in the received signal is focused outside the active region of the detector as in Figure 14b. This causes a corresponding increase in the BER as would be expected. Figures 14c and 14d help explain the case for decreasing BER with decreasing  $r_o$ . If the Airy disk is located off the active area of the detector near the edge, as in Figure 14c, during a period of large  $r_o$ , there will be either no signal or a very large BER because only some of the energy is being detected. As the size of the Airy disk increases due to decreasing  $r_o$ , part of the energy is seen by the detector as in Figure 14d and a corresponding drop in BER takes place.



Figure 14. Positioning of a Round Airy Disk on a Square Detector

The reason for the Airy disk being located outside the active detector region, as in Figure

14c, can be threefold. First, it can be a simple act of misalignment. by the operator. Since a great deal of care was taken in setting up the experiment to ensure a minimum BER and maximum signal-to-noise ratio at the receiver, the only reason for misalignment would be due to platform movement or atmospheric turbulence induced beam wander. The net result of the atmospheric turbulence and platform induced angle-of-arrival deviations determines the location of the Airy disk on (or off) the detector. We know these angle-of-arrival deviations are happening because when our  $r_o$  measurement system was developed, we not only gave it the ability to measure the diameter of the Airy disk, we also gave it the ability to keep track of where the disk is located on the CCD array and thus the ability to determine the angle-of-arrival of the incident radiation. Because of this ability, we have measured variations in angle of arrival as great as 0.15 degrees over a 24-hour period. This corresponds to a dislocation along the focal plane of approximately 250 pixels, or 1.7 millimeters over that period. Fifteen hundredths of a degree doesn't sound like much until you consider that the field-of-view of the telescope used to measure the  $r_o$  is only 0.6 degrees to begin with and the active area of the detector used for the communications receiver only has an active area diameter of 2 mm. Thus, if the alignment was initially set so that the Airy disk was in the center of the detector, it wouldn't be long before the energy of the incident radiation was escaping detection.

At this point, one might ask "Why not use a detector which has an active area large enough so that the system will work under all sizes of  $r_o$  and the full field-of-view of the optical system used to capture the incident radiation?" The answer is that as the area of the photodiode increases, so does the junction capacitance and the rise and fall times (diode speed decreases) and it becomes more susceptible to background noise. We initially used a photodiode with a 17mm diameter active region and the signal jitter was so great that the BERT would not sync to the signal except under nonturbulent conditions.

Visibility and platform movement are two factors that influence the BER extensively which cannot be ignored. Any airborne laser communication system will have to employ a built-in ac-

quisition and tracking system so the problems encountered with platform movement are not a factor. On the other hand, visibility, as determined by length of exposure, is a factor which is dependent upon the aerosols present along the communications path, the length of the path and divergence of the beam, and the amount of atmospheric turbulence present. The aerosols scatter and absorb the photons, and the atmospheric turbulence through the  $r_0$  defocuses the energy available at the detector, causing signal loss. Since the amount of time that our system requires to make an exposure is related to the amount of energy falling on the detector, it can be used to determine the visibility in a nonturbulent environment. However, in a turbulent environment, the amount of time required to make an exposure is dependent not only on the amount of energy present at the detector, but also the size of the resultant Airy disk. Therefore, in order to properly use the system as a device to measure the visibility, it would either have to be calibrated for use with a particular set of  $r_0$  values, or a model relating  $r_0$  and length of exposure to visibility would need to be developed. It does not appear as though  $r_0$  or visibility by themselves would make suitable single point predictors for determining the optimum communications parameters to be used for a minimum BER. However, length of exposure and  $r_0$  could potentially provide as much information as needed to make an intelligent decision as to the best parameters to use.

Although the MicroVAX graphics workstation with a VMS operating system and DEC windows is very user friendly, it is too large and too slow to meet the needs of a laser communications acquisition and tracking system. Personal computers (PC) have evolved to the point where they are fast (>50 MHz) and laptop computers are available with Liquid Crystal Displays (LCD) displays that have a high resolution 640 by 480 pixel capability. In addition, the newer laptops have expansion ports which will accept analog or digital frame grabbers. This will allow a much smaller, less expensive, faster, dedicated system to be put together. The high resolution video monitor is only required for the operator to provide a visual indication of the process. In an automated operational system, the monitor and hard disk logging could be eliminated

reducing the amount of software and time required to take a sample and make a decision, as well as reduce the size and weight of the system.

## 7 Future LCL Efforts

The algorithm which has been developed during this program to measure the diffraction limited aperture of the atmosphere can be expanded to control the communications process. With suitable interfaces, the computer can control the amount of gain supplied by the amplifier, the transmit power and beam divergence, data rate, and encoding. It could, if the system designer so desired, even be used to control the size of the aperture on variable aperture systems. Since it is more than likely that a CCD or CID array will be used in the acquisition and tracking process anyway, there is no reason why the acquisition and tracking algorithm couldn't be part of the algorithm that measures the  $r_0$  and apparent visibility, sharing the same computer resources. The result will be a computer based system which will monitor atmospheric turbulence, available energy, and tracking, and make adjustments as necessary to ensure optimum communications through a turbulent atmospheric environment.

Future in-house efforts in the LCL will incorporate the use of the system we developed to study/develop CCD based acquisition and tracking systems and adaptive laser communications systems. Plans are also under way to attack the received signal problem associated with scintillation to reduce/delete the frequency jitter in pulsed laser communications systems.

## 8 Summary

We set out in this project to develop a system which would be capable of monitoring the diffraction limited aperture of the atmosphere in the hope that we would some day be able to expand the system into an automated adaptive system which would sample the atmosphere and allow the computer to make an intelligent decision as to what the best modulation rate would be for an optimum communication channel. What we achieved is a system that is capable of measuring the  $r_0$  and the angle-of-arrival of the incident radiation and provide an indication of the visibility/incident energy. The best correlation coefficient of BER to  $r_0$  achieved during the test period was -0.68616 which means that more than 47% of the BER variance can be attributed to changes in the diffraction limited aperture of the atmosphere for our home-made laser communications system.

The UDC-500Q with a digital capability was the only frame grabber used for this project. The VIDEK camera mentioned above has a digital output which connects directly to the VIDEK input of the UDC-500Q. Each frame is captured and displayed completely. The UDC-500Q also requires a separate monitor for displaying the image. This is quite inconvenient when space is lacking. A better approach would be to use a frame grabber that uses the computer monitor for display.

We have attempted during this program to ascertain how free space laser communications using direct photodetection is affected by the presence of atmospheric turbulence, and the consequences of a small  $r_0$  and boundary layers in the atmosphere. By doing this, we hope to be able to gather enough insight into the problems of direct photodetection free space laser communications to develop an automated system which can adapt itself to obtain an optimum link in the presence of atmospheric turbulence. The data collected thus far clearly show that there are forces at work in the atmosphere which cannot be ignored. From this, it is obvious that a good laser communications system design depends not only on the diffraction limit of the optics used to focus the signal on to the detector, but also takes into account the diffraction limit of the

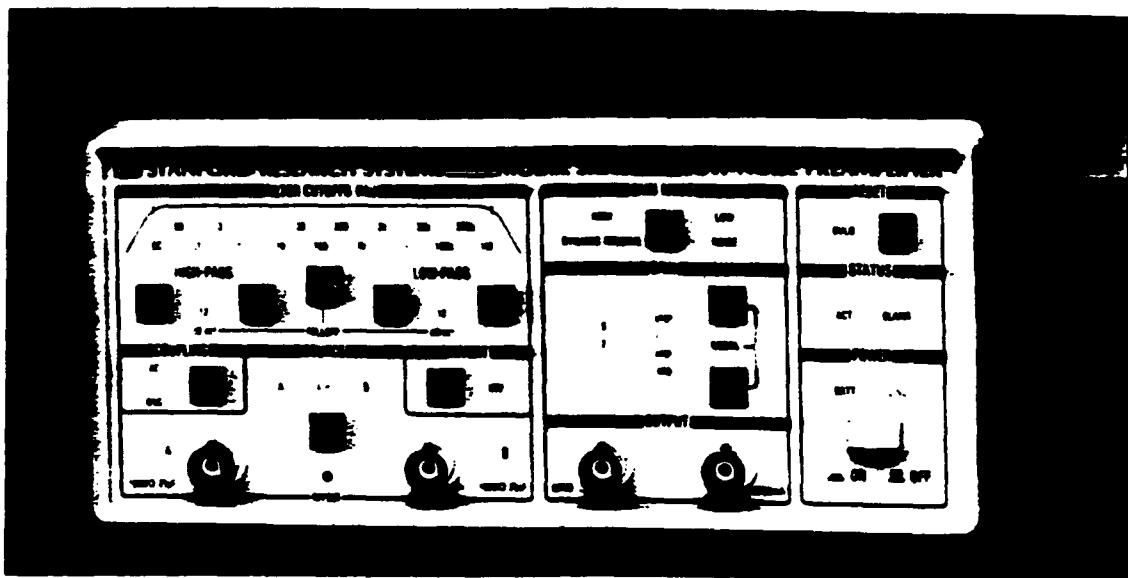


environment in which it is intended to be used.

## Appendix Equipment Specifications

# Low Noise Preamplifier

## Model SR560 - DC to 1 MHz Voltage Preamplifier



- 4 nV/√Hz Input Noise
- 1 MHz Bandwidth
- Variable Gain from 1 to 50,000
- AC or DC Coupled
- True Differential Or Single-ended Input
- 100 dB CMRR
- Two Configurable Signal Filters
- Selectable Gain Allocation
- Line or Battery Operation
- RS-232 Interface

### SR560 Overview

The SR560 is a high performance, low noise, general purpose preamplifier. With an input noise of only 4 nV/√Hz, a 1 MHz bandwidth, and a gain of up to 50,000, the SR560 is ideal for a wide variety of applications including low temperature measurements, optical detection, and audio engineering.

#### Signal Filters

Two configurable filters condition signals at frequencies from DC to 1 MHz. Choose flat, lowpass, bandpass, or highpass filtering to attenuate unwanted interference. Selectable gain allocation lets you further optimize performance for low noise or high dynamic reserve.

#### Intelligent Design

The microprocessor that runs the SR560 is "asleep" except during the brief interval it takes to change the

instrument's setup. This ensures that no digital hash will contaminate your low-level analog signals. You can change settings from the front panel or via the standard RS-232 interface. The RS-232 interface allows a single computer to control up to four SR560s. The RS-232 interface is optoisolated to further isolate the analog circuitry from any source of digital noise.

#### Line or Battery Operation

For complete isolation from the power line, the SR560 may be operated from its internal batteries for up to 15 hours. The battery voltage is regulated to ensure that amplifier performance is never degraded as the batteries discharge. Internal recharging circuits always maintain a fully charged battery when the unit is plugged into the line and automatic discharge detection circuitry prevents battery damage when the unit is left on with the batteries.

## LT-201

### PULSED LASER TRANSMITTER

- Featuring:
- \* 100 Watts Peak Optical Power
  - \* 904nm Wavelength
  - \* Beam Divergence 1mr
  - \* Operation up to 10KHz
  - \* Custom Units Available

Description: The LT-201 pulsed laser transmitter is intended to transmit short laser pulses through the atmosphere. This unit is well collimated and has a minimum optical output of 100 Watts. Utilizing the internal power supply repetition rates of 1.5KHz are achievable and with external power supplies repetition rates of 10KHz are achievable. These units are designed to be triggered externally.

#### Electro-Optical Characteristics at 25°C Case Temperature

	Min.	Typ.	Max.	Units
Peak Optical Output Power	100			Watts
Optical Pulse Width		40		ns
Maximum Repetition Rates -				
Internal Power Supply			1.5	KHz
External Power Supply		1	10	KHz
Wavelength		904		nm
Exit Aperture		50		mm
Beam Divergence		1		mr

Power Requirements = A Option - 12VDC  
                                  B Option - 24VDC

Trigger Input Requirements = 5 Volts into 50 ohms, 1 microsecond pulse width min. 5usec max.

Information provided by M/A-COM Laser Diode, Inc., is believed to be accurate and reliable. However, no responsibility is assumed for its use, or for infringement of the right of others.

M/A-COM Laser Diode, Inc., reserves the right to make changes at any time in order to improve the design and to supply the best product possible.

## MEGAPLUS Camera, Model 1.4

### Trigger Mode.

An external signal initiates the exposure. The Camera Control Unit terminates the exposure (as determined by the EXPOSURE switch setting) then transfers the image data to the host computer. This sequence is halted until another external signal is detected.

### Continuous Mode.

The Camera Control Unit self-initiates and terminates the exposure (as determined by the EXPOSURE switch setting), then transfers the image data to the host computer. This sequence is repeated indefinitely with no time gaps.

### Control Mode.

An external signal initiates then terminates the exposure (as determined by the time between the two states of the control line) then transfers the image data to the host computer. This sequence is halted until another external signal is detected.

### Sensor Specifications.

- Imaging Device: Solid-state charge-coupled device (CCD); full-frame imager.
- Total Pixels: 1,389,580 (1340 H x 1037 V).
- Light-sensitive Pixels: 1,363,095 (1317 H x 1035 V).
- Elements Transferred per Line: 1394 pixel clock pulses in each line transfer (1317 for active video + 77 for sync and blanking).
- Lines Transferred per Frame: 1037 (One dark line at the top and one dark line at the bottom)
- Pixel Size: 6.8 x 6.8 microns (square format).
- Center-to-Center Pixel Spacing: 6.8 microns, vertical and horizontal (unity fill-ratio).
- Active Area: 8.98mm (H) x 7.04mm (V). 4:3 aspect ratio; 2/3" format compatible.

### Video Performance.

- Black Level: Clamped to black reference at start of each line.
- Gamma: Unity.
- Scanning: Non-Interlaced.
- Synchronization: Internal.
- Dynamic Range: Greater than 55 dB at the Analog Video Output. Measured at an ambient temperature of <25°C, <50 msec exposure time and sampled synchronously with pixel clock.
- Pixel Clock Rate: 10 MHz.
- Frame Rate: 6.9 frames/sec. @ strobe illumination.  
5.1 frames/sec. @ 50 msec exposure time.  
2.5 frames/sec. @ 250 msec exposure time.

Note: Frame Rate = 1/(145 milliseconds + exposure time)

Specifications subject to change without notice.

### Mechanical Specifications.

#### Camera Head

All aluminum gasket sealed case.

Dimensions:

- F-Mount: 4.45" x 3.90" x 5.19"
- C-Mount: 4.45" x 3.90" x 4.69"
- Weight: 3 lbs
- Tripod Mount: 1/4 - 20 threads.

#### Camera Control Unit

- Dimensions: 2.51" x 12.0" x 9.94"
- Weight: 6 lbs
- Mounting: Feet for desktop, brackets for hard mounting in any orientation.

### Environmental Requirements.

#### Temperature

- Operating: 0 to 35° C (32 to 95° F), non-condensing (Image quality will degrade with increasing temperature).
- Storage: -25 to +80° C (-13 to 176° F), non-condensing.

#### Humidity

- Operational: < 80% @ 40° C (95° F).
- Storage: < 40% @ 80° C (176° F).

**Vibration:** 3 g, sinusoidal from 5 to 150 Hz.

**Shock:** 20g.

# UDC-500Q Series

**Video Digitizer & Dual Frame  
Display Controller for Q-Bus**

## FEATURES

### MEMORY

- Dual Frame Buffers up to 1024 x 1024 x 8-bits each
- Overlay memory-1024 x 1024 x 2-bits
- 1/4 MBytes of Display List
- Dual Ported Memory

### DISPLAY

- Up to 1024 x 1024 x 8-bit Display Resolution
- 256 Colors or Gray Levels
- 1024 x 1024 x 2-bit graphic overlay
- Hardware pan, scroll, zoom
- Flicker-free 60 Hz non-interlaced display
- Input and Output LUT's
- Using 82786 GPU Graphic Controller

### VIDEO INPUT (Optional)

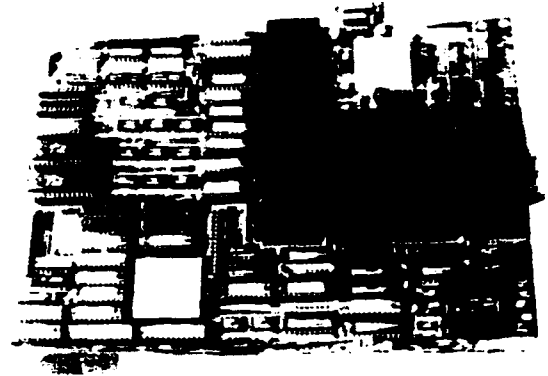
- Video Digitizer accepts any standard or non-standard analog or digital video inputs up to 1024 x 1024 @ 15 Hz, 30 Hz or 60 Hz interlaced or non-interlaced

### FUNCTIONAL

- Occupies single quad-size Q-bus slot
- Supplied with initialization and diagnostic software
- Callable imaging and graphics library software available

## TYPICAL APPLICATIONS

- Medical imaging
- CAD/CAE
- Animation
- Landsat Image Analysis



## GENERAL DESCRIPTION

The UDC-500 is an advanced high resolution dual frame bit-mapped display controller featuring input video digitizers which can digitize analog or digital input sources up to 1024 x 1024 @ 15, 30 or 60 Hz interlaced or non-interlaced. It can also display 256 colors from a palette of over 16.4 million.

By combining the Intel 82786 display controller with video RAM memory, operations such as polygon drawing, line drawing, bit block transfers, and multi-font text generation are performed at high speeds. The display/overlay memory is dual ported thus allowing high speed host access. In addition, the display memory is double buffered enabling one buffer to be displayed while the other is being updated by the graphic processor or the video digitizer. On board logic controls the selection of the display buffer in real time without host intervention or flicker.

The product is configured on a single DEC quad-sized Q-bus compatible card with the optional input video digitizer provided as a plug-in daughter board. The unit is provided with a Micro VMS-compatible initialization and diagnostic software. Other drivers and a software library are also available.

# PRODUCT SPECIFICATIONS

## Performance Characteristics

Display Mode	Landscape
Bit Map Memory	2 MBytes Frame Buffer 256KBytes Display list 256KBytes Overlay
Display Resolution	1024 x 1024 x 8-bit
Zoom Factor	2:1, 4:1
Output LUT	provided
Video Bandwidth	87 MHz
Monitor Scan Rate	up to 64 KHz 60 Hz non-integrated
Host Interface	DEC MicroVAX Occupies a single quad slot
Memory Access	Byte, word two pixels per access from the host Bus at 2 Million pixels/sec.
Register Access	Memory mapped
Memory Addressing	Memory mapped

## High Speed Drawing Functions

Line, Polygon, Arc, Circle, Fast Bit Block Copies, Text, Multi-horizontal Split Screens Hardware Clipping, Boolean read modify write drawing commands

Video output	RS-343 Composite or separate sync
--------------	--------------------------------------

## (Optional) Video Digitizer Inputs

Digital Version	Direct digital interface from VIDEK Megaplus camera (or similar)
Analog Version	8-bit flash A.D Converter operating at 10 or 20 MHz
Resolution	Programmable up to 1024 x 1024 interlaced or non-interlaced
Input LUT	provided
DC restoration	provided
Input Video BW	21 MHz

## Mechanical Characteristics

Dimensions	Occupies 1 MicroVAX Q-bus slot 2 slots with option 510 8.43" x 10.46" single board
Oper. Temp.	0 to +70°C
Relative Humidity	0 to 90% non-condensing
Warranty	1 year factory parts and labor
Monitors Supported	Hitachi, Panasonic, SONY, Mitsubishi, others (consult factory)

Specifications subject to change without notice.

DEC, Q-Bus, and MicroVAX are registered trademarks of Digital Equipment Corporation.

## Ordering Information

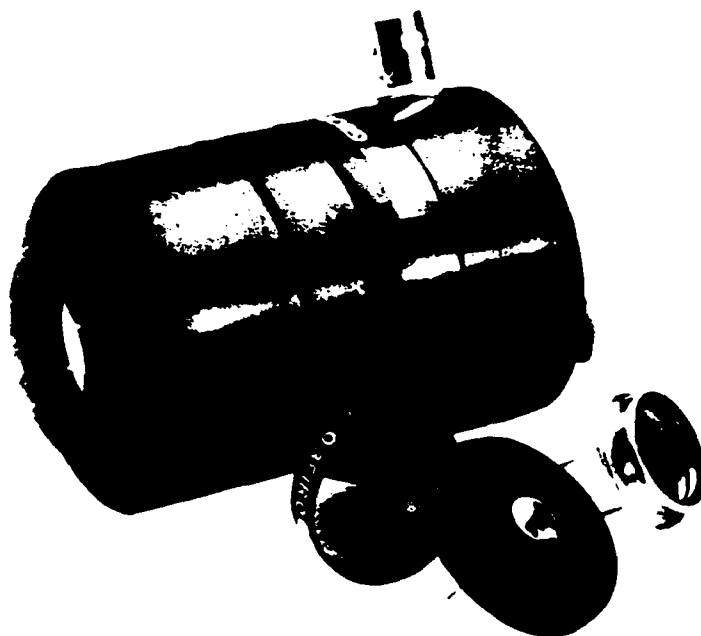
UDC-500-Q 10M	1024 x 1024 x 8-bit monochrome dual frame buffer
UDC-500-Q 10C	1024 x 1024 x 8-bit color dual frame buffer

### OPTIONS

UDC-501	digital digitizer input
UDC-510	analog digitizer input
UDC-511	both analog and digital digitizers

# ▶ Photodetection System

For Collimated and Near-Collimated Radiation



*New from Melles Griot, a modular system for light detection consisting of photodiodes, photodiode mounts, and optical filters for light detection from 350nm to 1100nm.*

## MOUNTS

### ▶ Universal Modular Photodiode Mount

Photodiodes may be quickly mounted or replaced. Electrical connection is made using sleeved clips, eliminating the need to solder and unsolder photodiode leads

System provides convenient mounting for TO5, TO8, TO46 and TO75 style photodiodes

A BNC socket provides a simple electrical interface to amplifiers and sensing circuits

### ▶ Stackable, Snap-together Filter Mounts

Easy snap-action mounting mechanics for addition or substitution of optical filters, 25mm or 1 inch in diameter

## SILICON PHOTODIODES

NIST (formerly NBS) traceable calibration services from 350nm to 1100nm

Low dark current minimizes signal noise

### Applications Include:

*Laser Beam Sensing*

*Photometry and Radiometry*

*Analytical Instrumentation*

*Process Control Instrumentation*

*Optical Communications*

## OPTICAL FILTERS

▶ **Neutral Density Filters** — prevent photodiode saturation by attenuating the incident light beam

▶ **Bandpass Filters** — eliminate noise present in a photodiode's output signal due to background lighting

▶ **Opal Glass Diffuser** — reduces the signal amplitude error of photodiodes caused by non-uniformity and spatial drifting in the incident light beam



# UNIVERSAL MODULAR MOUNTING SYSTEM FOR PHOTODIODES

The Melles Griot modular mounting system for photodiodes, eliminates the three most common problems associated with using photodiodes in optical systems, namely, mounting the detector, connecting it to an operating and sensing circuit, and providing a convenient user interface to optical filters.

Designed for quick installment or replacement of a photodiode in an optical system, the Universal Detector Mount (13 DMA 001) holds the photodiode in a very stable mounting position. Four adaptor rings are included which accept a variety of photodiode can styles, including TO5, TO8, TO46 and TO75. Electrical connection to the detector is made

using sleeved clips, eliminating the need for soldering and unsoldering leads. A BNC socket is included for a convenient interface to an external sensing circuit or amplifier.

The Melles Griot Stackable Filter Mounts (13 DMA 003 and 13 DMA 005) are accessories to the Universal Detector Mount. Together, they create a light-tight mounting system which completely blocks stray ambient light (thereby reducing background noise) and makes adding or substituting optical filters in front of the photodiode easy. Mounts simply "snap" together, and accommodate filters either 25mm or 1 inch in diameter.

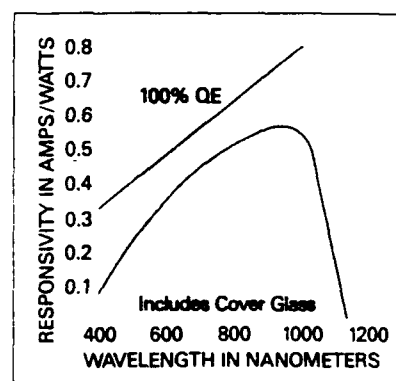
PRODUCT NUMBER	A	øB
13 DMA 001	39.7	50
13 DMA 003	19.8	50
13 DMA 005	27.0	50

## SILICON PHOTODIODES

New from Melles Griot, single element planar diffused photodiodes are designed for general purpose, medium to high speed light detection applications. Each device consists of a silicon photodiode element mounted in a sealed metal can with a thin cover glass. This ensures mechanical ruggedness and reliable operation. As a result of a carefully controlled diffusion process, Melles Griot 13 DSI series photodiodes exhibit characteristically low dark current, high linearity, and operate over a wide spectral range (see graph). This allows accurate detection of very low light levels across the visible and into the near-IR.

In certain applications where the measurement of absolute light levels is imperative (particularly various types of radiometry), a photodiode's typical responsivity may not be sufficient. In these instances it is necessary to use a detector whose absolute responsivity has been

accurately characterized. Melles Griot offers full responsivity calibration and re-calibration services from 350nm to 1100nm on the following silicon photodiodes: 13 DSI 007, 13 DSI 009 and 13 DSI 011. The photodiode calibration services are traceable to NIST (formerly NBS) standards.

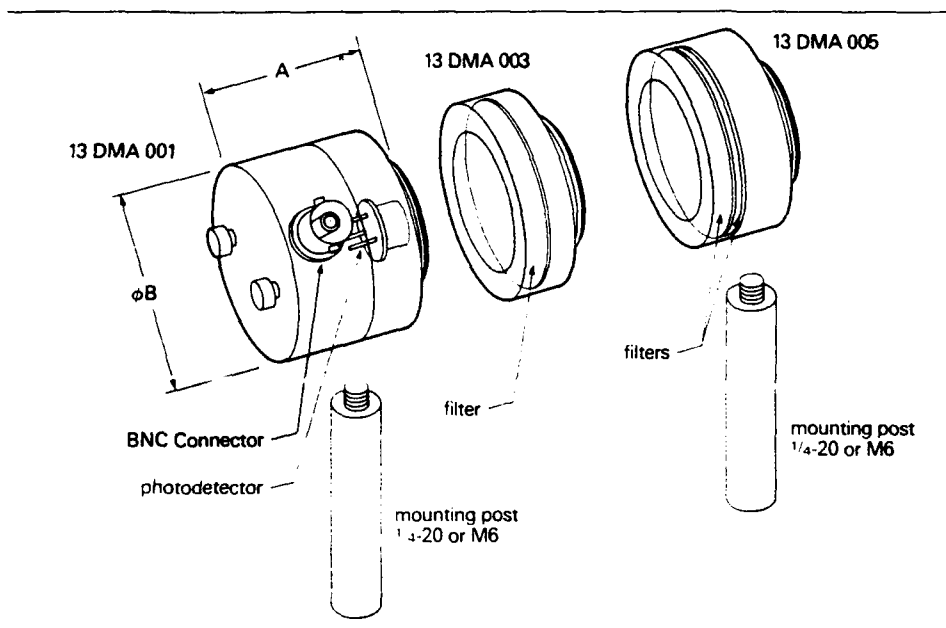


### SPECIFICATIONS

**Spectral Response Band:** 350-1100 nanometers

**Responsivity:** 0.45 Amps/Watt @ 830 nanometers minimum, no cover

Active Area (mm <sup>2</sup> )	Dark Current V <sub>rb</sub> @ 1V (nA)	Voltage Breakdown (V)	Shunt Resistance V <sub>rb</sub> = 0 (MΩ)	Junction Capacitance V <sub>rb</sub> = 0 (pF)	NEP @ 830nm (25°C) (W √ Hz <sup>-1</sup> )	Package Type	PRODUCT NUMBER
0.31	0.7	60	300	10	$1.5 \times 10^{-14}$	TO46	13 DSI 001
1.00	0.9	40	120	25	$2.3 \times 10^{-14}$	TO46	13 DSI 003
3.10	3.1	30	60	72	$3.3 \times 10^{-14}$	TO5	13 DSI 005
10.00	10.0	20	40	230	$4.1 \times 10^{-14}$	TO5	13 DSI 007
31.00	31.0	15	10	713	$8.1 \times 10^{-14}$	TO8	13 DSI 009
100.00	110.0	10	4	2300	$1.3 \times 10^{-13}$	TO75	13 DSI 011



## PHOTODETECTION SYSTEM PERFORMANCE

A typical light detection system consists of a photodiode and its associated sensing circuit (load). This circuit largely influences the bandwidth the system will have, and the minimum optical power the system can accurately detect. System performance is based upon the selection of photodiode and load type (amplifier, resistive load) for a given application.

An important consideration when selecting a photodiode is the size of

the device's active area. Photodiodes with larger active areas, e.g.  $31\text{mm}^2$  and  $100\text{mm}^2$ , are useful for applications requiring an extended field of view, or the measurement of expanded beams of light. However, there is a design trade-off with increased noise. Photodiodes with small active areas, e.g.  $0.31\text{mm}^2$  to  $3.1\text{mm}^2$  are less noisy and well suited for very directional measurements, but usually require optics to focus the incoming light. This presents a variety of mounting and positioning choices.

Shown below is a table indicating the combined system performance for Melles Griot's new silicon photodiodes and the new transimpedance amplifier (13 AMP 003). Once an applications bandwidth and signal-to-noise requirements have been identified, this table will be useful for identifying the appropriate photodiode/amplifier combination.

PHOTODIODE PRODUCT NUMBER	BANDWIDTH (kHz)			CURRENT NOISE (Amps RMS)			NEP (Watts RMS)		
	Amplifier Gain (Volts/Amp)			Amplifier Gain (Volts/Amp)			Amplifier Gain (Volts/Amp)		
	$10^3$	$10^6$	$10^9$	$10^3$	$10^6$	$10^9$	$10^3$	$10^6$	$10^9$
13 DSI 001	45	35	0.1	$2.0 \times 10^{-8}$	$9.8 \times 10^{-11}$	$7.1 \times 10^{-13}$	$4.4 \times 10^{-8}$	$2.2 \times 10^{-10}$	$1.6 \times 10^{-12}$
13 DSI 003	45	35	0.1	$2.0 \times 10^{-8}$	$1.2 \times 10^{-10}$	$7.9 \times 10^{-13}$	$4.4 \times 10^{-8}$	$2.7 \times 10^{-10}$	$1.8 \times 10^{-12}$
13 DSI 005	45	35	0.1	$2.0 \times 10^{-8}$	$1.5 \times 10^{-10}$	$9.0 \times 10^{-13}$	$4.4 \times 10^{-8}$	$3.3 \times 10^{-10}$	$2.0 \times 10^{-12}$
13 DSI 007	45	35	0.1	$2.0 \times 10^{-8}$	$2.6 \times 10^{-10}$	$1.4 \times 10^{-12}$	$4.4 \times 10^{-8}$	$5.8 \times 10^{-10}$	$3.1 \times 10^{-12}$
13 DSI 009	45	35	0.1	$2.0 \times 10^{-8}$	$5.7 \times 10^{-10}$	$2.3 \times 10^{-12}$	$4.4 \times 10^{-8}$	$1.3 \times 10^{-9}$	$5.1 \times 10^{-12}$
13 DSI 011	45	35	0.1	$2.0 \times 10^{-8}$	$1.2 \times 10^{-9}$	$3.5 \times 10^{-12}$	$4.4 \times 10^{-8}$	$2.7 \times 10^{-9}$	$7.8 \times 10^{-12}$

The table shows the combined performance for Melles Griot Silicon Photodiodes and Transimpedance Amplifier 13 AMP 003. NEP values for a responsivity of 0.45 Amps/Watt.

## WIDE BANDWIDTH DETECTOR AMPLIFIER 13AMP005

The Melles Griot Wide Bandwidth Amplifier (13AMP005) is a high speed, DC-coupled, transimpedance amplifier. It is intended for use with photodiode detectors, including silicon, germanium, and AlGaAs devices. The amplifier has a useful range of input currents from 100pA to 2mA in five gain ranges. The input current is displayed on the front panel LCD. The unit provides a settable detector reverse bias voltage for improving detector response time. It also has an offset current adjustment for nulling background currents.



### FEATURES

- **TRANSIMPEDANCE GAIN**  
*Amps to Volts conversion*
- **FIVE DECADE GAIN RANGE**  
1,000 to 10,000,000 V/A
- **WIDE BANDWIDTH**  
DC to 5MHz at 1,000V/A
- **LCD DISPLAY**  
3 1/2 digit LCD with backlight
- **LOW NOISE**  
100nA RMS, at 1,000 V/A  
20pA RMS, at 10,000,000 V/A
- **ADJUSTABLE BIAS**  
-10V to +10V

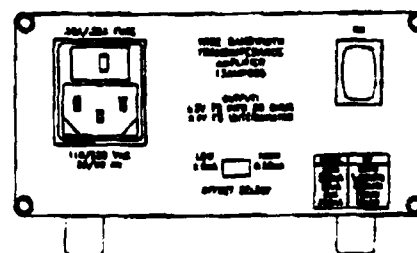
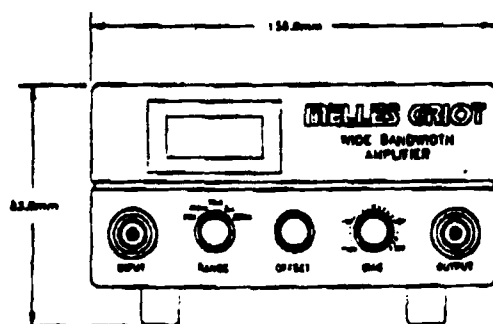
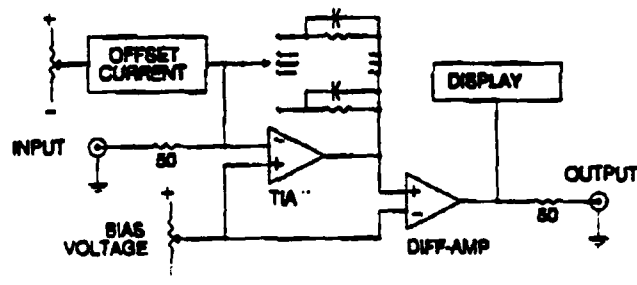
### APPLICATIONS

- Air-to-air optical communications
- Fiber-optic communications
- Detector characterization
- Laser pulse detection
- Industrial beam interrupt detection
- Radiometric calibration

Input	-2mA to +2mA
Input Connector Type	BNC
Output	-2V to +2V (-4V to +4V unterminated)
Output Impedance	50 Ohms
Output Connector Type	BNC
Bias Voltage Range	$\pm 10V$
Offset Current Range	$\pm 5\mu A$ (Low), $\pm 50\mu A$ (High)
Display Range	-1.999 to +1.999
Dimensions	83mm H x 136mm W x 178mm D
Weight	1.13Kg
Power Requirements	100-120/220-240 VAC, 50-60 Hz, 10 Watts maximum
Operating Temperature	+10°C to +35°C
Storage Temperature	-40°C to +55°C

GAIN (V/A)	BANDWIDTH (-3db)	RMS NOISE (5MHz BW)
1,000	5 MHz	100 nA
10,000	1.25 MHz	12 nA
100,000	300 KHz	1.5 nA
1,000,000	75 KHz	180 pA
10,000,000	15 KHz	22 pA

\* Specifications subject to change without notice.



9034-A

## Bibliography

### Conference and Technical Reports:

1. Andrews, Harry C., Tutorial and Selected Papers in Digital Image Processing, (various authors), IEEE Inc., New York, NY 1978.
2. Tai, A., Eisman, M. and Neagle, B., "Holographic Lens for Wide FOV Laser Receiver," Computer and Optically Formed Holographic Optics, Ivan Cindrich, Sing H. Lee, Editors, Proc. SPIE 1211, pp. 238-246 (1990).
3. Wilkins, Gary D., "Measurement of the Atmospheric Phase Coherence Length,  $r_0$ ," In-house report RADC-TR-86-192, December 1986.

### Textbooks:

1. Barnoski, Michael K., Fundamentals of Optical Fiber Communications, New York, Academic Press, Inc., 1976.
2. Cathey, W. Thomas, Optical Information Processing and Holography, New York, John Wiley and Sons, 1974.
3. Dereniak, Eustace L. and Crowe, Devon G., Optical Radiation Detectors, New York, John Wiley and Sons, 1984.
4. Gagliardi, Robert M. and Karp, Sherman, Optical Communications, New York, John Wiley and Sons, 1976.
5. Goodman, Joseph W., Introduction to Fourier Optics, New York, McGraw-Hill Book Co., 1968.
6. Goodman, Joseph W., Statistical Optics, New York, John Wiley and Sons, 1985.
7. Green, William B., Digital Image Processing: A Systems Approach, New York, Van Nostrand Reinhold, 1989.
8. Hall, Ernest L., Computer Image Processing and Recognition, New York, Academic Press, Inc., 1979.
9. Hecht, Eugene, Optics, Massachusetts, Addison-Wesley Publishing Co, 1990.
10. Yaroslavsky, L. P., Digital Image Processing, New York, Springer-Verlag, 1985.